ELSEVIER

Chemical Engineering Journal 74 (1999) 171–179

Chemical Engineering Journal

Dynamics of pressure build-up accompanying multicomponent gas transport in porous solids: adsorbable gases

Vladimír Hejtmánek*, Pavel Čapek, Olga Šolcová, Petr Schneider

Institute of Chemical Process Fundamentals, Academy of Sciences of the Czech Republic Rozvojová 135, 165 02 Praha 6-Suchdol, Czech Republic

Received 14 September 1998; received in revised form 11 February 1999; accepted 11 February 1999

Abstract

The dynamics of countercurrent transport of binary and ternary gas mixtures, containing one absorbable gas, through a porous medium accompanied by a spontaneous temporary build-up of pressure inside the pores was experimentally studied. Attempts to simulate the pressure responses based on Maxwell–Stefan constitutive equation (2) were made with the conclusion that adsorption in equilibrium overpredicts the temporal pressure inside the porous solid. To simulate acceptably pressure responses for the porous catalyst ICI-52/1 adsorption kinetics must be considered.

Keywords: Dynamic transport; Multicomponent; Transport parameters; Mean transport pore model; Dusty-gas model

1. Introduction

Recently we have reported about spontaneous pressure changes which accompany combined (diffusion and permeation) transport of binary and ternary gas mixtures through a porous industrial catalyst ICI-52/1 under dynamic conditions [1,2].

Pressure change following a step change in gas composition was monitored in a cell schematically shown in Fig. 1. The studied cylindrical porous pellets were mounted in cylindrical holes of an impermeable metallic disk, which separated the upper flow-through compartment from the closed lower compartment. The closed compartment was equipped with a sensitive pressure transducer. By flowing a gas (or gas mixture) A through the upper compartment, before the start of measurement, both compartments were filled with A. At the measurement start the gas (or gas mixture) A in-flow into the upper compartment was step-wise replaced by gas (or gas mixture) B (denoted as B→A[1]; if both gases were reversed A→B). Pressure in the upper compartment was kept constant at all times. Output of the pressure transducer was followed until the pressure before the measurement start was restored.

Different gases or gas mixtures were selected from the set of four inerts: hydrogen, helium, nitrogen, and argon. It was shown that the mean transport pore model (MTPM) and the dusty gas model (DGM) could satisfactorily describe the spontaneous temporary pressure build-up. Both models contain three parameters (transport parameters) which represent material constants of the porous medium, i.e. are independent of the kind of transported gases and conditions under which the transport takes place (temperature, pressure). These parameters have been determined by matching of experimental pressure response to theoretical model predictions.

It is the aim of this contribution to verify:

1. if the combined transport of gas mixtures containing adsorbable gases is followed by a spontaneous temporary pressure build-up similar as with inert gases and
2. if the MTPM and DGM models with transport parameters optimal for inert gases can simulate the pressure responses.

The cell shown in Fig. 1 working at room temperature and in the upper compartment at atmospheric pressure was employed in all experiments. The same porous catalyst ICI-52/1 as in the study of inert gases was used. Methane, ethane, propane and *n*-butane were used as adsorbable gases and hydrogen and nitrogen as inerts. Langmuir adsorption isotherms of methane, ethane, propane and *n*-butane were determined with the Cahn vacuum microbalance.

*Corresponding author. E-mail: hejtmanek@icpf.cas.cz (V. Hejtmánek)

1385-8947/99/$ – see front matter
PII: S1385-8947(99)00078-9

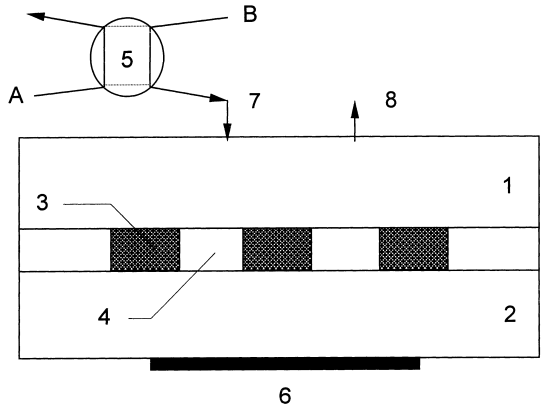

Fig. 1. Scheme of the measuring cell: (1) upper compartment, (2) lower compartment, (3) porous pellets, (4) impermeable disk, (5) four-way valve, (6) pressure transducer, (7) cell inlet, (8) cell outlet.

2. Experimental

2.1. Porous catalyst

Cylindrical pellets (height/diameter=3.81/5.50 mm) of a commercial hydrogenation catalyst from Imperial Chemical Industries ICI 52/1 (CuO+ZnO/alumina) in the unreduced form was used. Textural properties of the tested catalyst are summarized in Table 1. From the pore-size distribution (Fig. 2) obtained by a combination of mercury porosimetry (AutoPore 9200, Micromeritics, USA) and low temperature nitrogen adsorption (ASAP 2010M, Micromeritics, USA) can be seen that the catalyst is monodisperse with the most frequent pore diameter of 16.4 nm.

2.2. Gases

Gases (hydrogen, nitrogen, methane, ethane, propane and *n*-butane; Linde Co.) from pressure cylinders had the 99.9% purity.

2.3. Diffusion cell (Fig. 1)

48 cylindrical pellets of lCl 52/1 were fastened into the holes of the metallic disk by forcing them first into an undersized silicon rubber tube and then forcing the pellet-rubber tube assembly into the hole.

The pressure transducer (4-API-50; Jumo Wien, Austria) responded linearly in the pressure range −100 to +50 kPa. The volume of the lower compartment was minimized (10.2 cm^3) to achieve shortening of the responses. The volume of the upper compartment was 9.1 cm^3. Mass flow-meter controllers adjusted the flow rates of gases entering the upper compartment. A four-way valve was used for switching of gases entering the upper compartment. The gas flow rate in the upper compartment was maintained at 1.3 cm^3/s.

Readings from the pressure transducer were stored in a computer as time dependence of relative pressure $p_{rel}=p/p_b$ (with atmospheric pressure p_b).

The dynamic runs were accomplished with binary and ternary mixtures of inert and adsorbable gases.

Table 1
Textural properties of catalyst ICI 52/1

Specific surface	73 m^2/g
Skeletal density	3.833 cm^3/g
Apparent density	1.518 g/cm^3
Pore volume	0.377 cm^3/g
Porosity	0.604
Mean pore diameter	16.4 nm

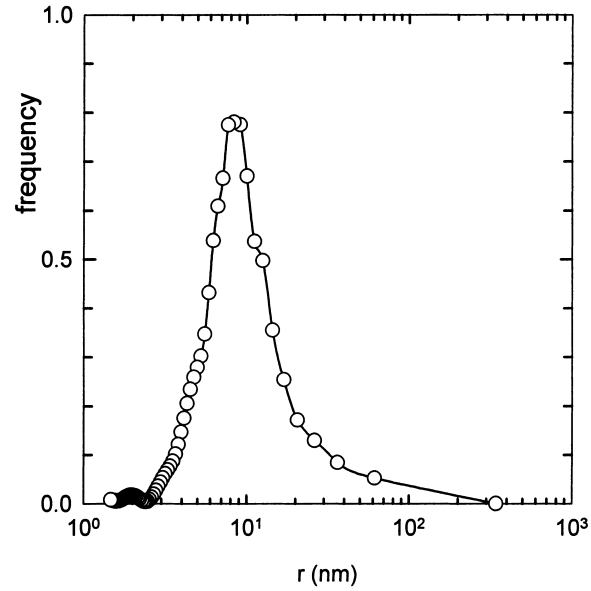

Fig. 2. Pore size distribution of ICI 52/1.

2.4. Adsorption measurements

Adsorption isotherms were determined at atmospheric pressure and 25°C under steady-state conditions by gravimetric method with the Cahn vacuum microbalance (D-2000, Cahn Instruments, USA). The hydrocarbon streams were diluted by nitrogen to obtain different hydrocarbon partial pressures. The obtained isotherms are shown in Fig. 3. Parameters of the Langmuir adsorption isotherms (1) (adsorption capacities, q_{max}, adsorption equilibrium constants, K_i) are summarized in Table 2.

Table 2
Parameters of Langmuir adsorption isotherms

Hydrocarbon	Adsorption capacity q_{max} (mmol/g)	Adsorption constant K (cm^3/mmol)
Methane	0.40 [a]	0.0054 [a]
Ethane	0.40	4.3
Propane	0.37	21.0
n-Butane	0.44	89.4

[a] Estimated by assuming q_{max}(methane)=q_{max}(ethane)=0.40 mmol/g.

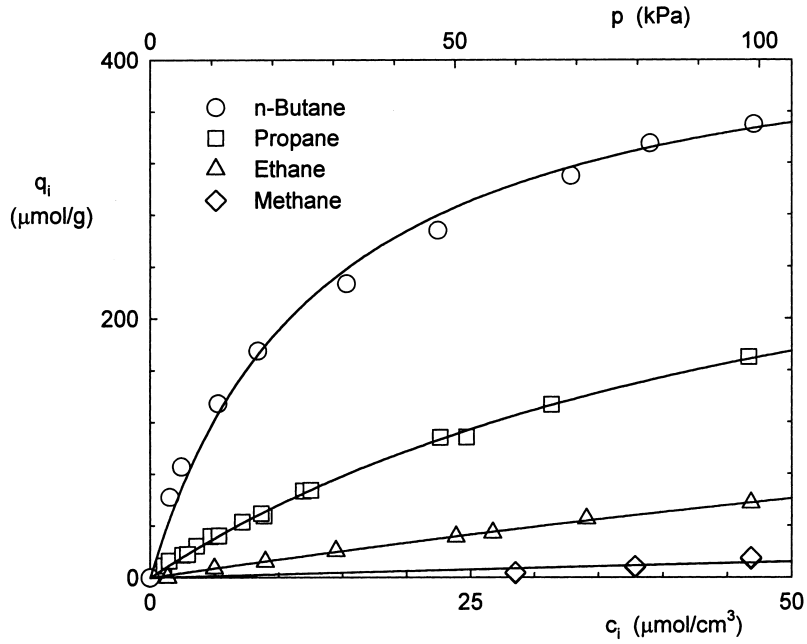

Fig. 3. Adsorption isotherms of methane, ethane, propane and *n*-butane.

$$q_i = \frac{q_{\max} K_i c_i}{1 + K_i c_i}, \quad (1)$$

whereas adsorption capacities are similar for all the investigated hydrocarbons, the adsorption equilibrium constant of *n*-butane is about twenty times higher than that of ethane and four to five times than that of propane. Adsorption of methane was so low that even at atmospheric pressure it was in the Henry region; hence only the product $q_{\max}K$ could be determined (0.0022 cm^3/g). When the adsorption capacity for methane is assumed to be the same as for ethane the methane adsorption equilibrium constant K=0.0054 cm^3/mmol was obtained.

3. Theoretical

Two models of porous structure are available in the literature for description of the combined transport of multicomponent gas mixtures, viz. the mean transport pore model (MTPM [3,4]) and dusty gas model (DGM [5]). Both models are based on the modified Maxwell–Stefan diffusion equation and the Darcy equation describing the permeation flow, i.e. flow under total pressure gradient. The Maxwell–Stefan diffusion equation accounts for diffusive transport in the transition region between the Knudsen region and bulk region. In MTPM the composition gradient (mole fraction gradient) is taken as the diffusion driving force. DGM assumes that diffusion is driven by concentration gradient (gradient of molar concentrations). The permeation equation in the form of Darcy law can take into account either only the Poiseuille viscous flow (DGM), or, combined Knudsen flow, slip at the pore wall and the Poiseuille viscous flow (MTPM: Weber equation [3,12]).

3.1. Models describing combined multicomponent gas transport in pores

3.1.1. Mean transport pore model

Mean transport pore model assumes that the decisive part of the gas transport takes place in transport pores that are visualized as cylindrical capillaries with radii distributed around the mean value $\langle r \rangle$. The width of this distribution is characterized by the mean value of the squared transport pore radii, $\langle r^2 \rangle$. The last model parameter is the ratio of porosity, ϵ_t, and tortuosity of transport pores, q_t, $\Psi = \epsilon_t/q_t$. Transport parameters appear always as combinations: Ψ (effective porosity of transport pores), $\langle r \rangle \Psi$ (effective transport pore radius) and $\langle r^2 \rangle \Psi$ (effective viscous flow parameter). These parameters represent material properties of porous solid related to mass transport, and thus, do not depend on temperature, pressure, and kind of the transported gases. They have to be determined experimentally, preferentially with inert gases.

3.1.2. Dusty gas model

Dusty gas model visualizes the porous medium as a collection of giant spherical molecules (dust particles) kept in space by external force. The movement of gas molecules in the spaces between dust particles is described by the kinetic theory of gases. Formally, the MTPM transport parameters Ψ, $\langle r \rangle \Psi$ and $\langle r^2 \rangle \Psi$ can be used also in DGM.

3.2. Maxwell–Stefan constitutive equation

The dusty gas model (DGM) and mean transport pore model (MTPM) are based on the Maxwell–Stefan theory. Both models include contributions of bulk diffusion, Knud-

sen diffusion and permeation flow that accounts both for viscous flow, and Knudsen flow (MTPM includes also the slip at the pore wall). The vector form of the relation between molar flux densities, $\mathbf{N}=\{N_1, N_2,\ldots, N_n\}^T$, and gradients of molar concentrations, $\mathbf{c}=\{c_1, c_2,\ldots,c_n\}^T$, is the same for both models

$$\mathbf{H}(\mathbf{c})\cdot\mathbf{N}+\frac{\partial\mathbf{c}}{\partial x}=0, \tag{2}$$

where $\mathbf{H}(\mathbf{c})$ is a square $(n\times n)$ concentration dependent matrix (for matrix elements, h_{ij}, see Appendix A). This matrix hides [4] the differences between both models. The matrix elements depend on transport properties of pure gases and their binary mixtures, and on the structure of the porous solid (characterized by three parameters Ψ, $\langle r\rangle\Psi$ and $\langle r^2\rangle\Psi$).

3.3. Mass balance of measuring cell

Mass balances for an n component gas mixture with the first m gases adsorbable ($m\leq n$), inside the porous pellets, supplement the constitutive Eq. (2)

$$\epsilon\frac{\partial\mathbf{c}(t,x)}{\partial t}+\rho_p\frac{\partial\mathbf{q}(t,x)}{\partial t}=-\frac{\partial\mathbf{N}(t,x)}{\partial x}, \tag{3}$$

where ϵ is the total pellet porosity, ρ_p the apparent pellet density and t time. Here $\mathbf{q}$ is the vector (of length n) of adsorbed amounts augmented by zeroes for nonadsorbable species, $\mathbf{q}=\{q_1, q_2,\ldots,q_m, 0, 0,\ldots,0\}^T$. Boundary conditions of the system of partial differential Eqs. (2) and (3) follow from the mass balance of both compartments assuming no resistance to mass transport between the bulk gas and the pellet.

3.4. Accumulation of adsorbed species

The accumulation of adsorbed species, $\partial\mathbf{q}/\partial t$, can be formulated for different situations.

When *adsorption* of all adsorbable components is in *equilibrium* described by the multicomponent Langmuir adsorption isotherm:

$$q_i=\frac{q_{\max}K_ic_i}{1+\sum_{j=1}^m K_jc_j}, \tag{4}$$

then

$$\frac{\partial q_i}{\partial t}=\sum_{j=1}^m\frac{\partial q_i}{\partial c_j}\frac{\partial c_j}{\partial t}=\sum_{j=1}^m\frac{q_{\max}K_i\left[\left(1+\sum_{j=1}^m K_jc_j\right)\delta_{ij}-K_jc_i\right]}{\left(1+\sum_{j=1}^m K_jc_j\right)^2}\frac{\partial c_j}{\partial t},$$
$$i=1,\ldots,m \tag{5}$$

with δ_{ij}, the Kroneker delta.

With adsorption kinetics:

$$\frac{\partial q_i}{\partial t}=k_i\left[c_i\left(q_{\max}-\sum_{j=1}^m q_j\right)-\frac{q_i}{K_i}\right], \tag{6}$$

where k_i is the adsorption rate constant of component i.

3.5. Boundary conditions

If ideal mixing is assumed at $x=L$ (lower compartment), the condition has the form

$$V_L\frac{\partial\mathbf{c}(t,L)}{\partial t}=S\mathbf{N}(t,L), \tag{7}$$

where V_L is the free volume of the lower compartment, S the total cross-section of cylindrical pellets in the metallic disk and L is their length.

At $x=0$ (upper compartment) the boundary conditions are

$$V_U\frac{\partial\mathbf{c}(t,0)}{\partial t}=F^0\mathbf{c}^0-F\mathbf{c}(t,0)-S\mathbf{N}(t,0), \tag{8}$$

where F^0 and F are the volumetric gas flow rates at the upper compartment inlet and outlet, respectively, and V_U is the upper compartment volume. Eq. (8) again assumes ideal mixing in the compartment. The unknown outlet volumetric flow rate, F, in Eq. (8) is obtained from the overall mass balance

$$F=F^0-S\frac{\sum_{i=1}^n N_i(t,0)}{\sum_{i=1}^n c_i(t,0)}. \tag{9}$$

3.6. Initial conditions

Initial conditions for the system of Eqs. (2), (3), (5)–(9) are formulated as

$$\mathbf{c}(0,x)=\mathbf{c}^* \tag{10}$$

with the vector of constant component concentrations, $\mathbf{c}^*=\{c_1^*, c_2^*,\ldots, c_n^*\}^T$, determining the equilibrium state when the cell is completely flushed by a single gas or gas mixture.

In addition, for the case with adsorption kinetics (i.e. the system (2), (3), (6), (7)–(9)) initial adsorbed amounts $\mathbf{q}(0,x)=\mathbf{q}^*$ follow from the adsorption equilibrium (4)

$$q_i=q_i(c_1^*, c_2^*,\ldots, c_m^*). \tag{11}$$

3.7. Solution method

The system of Eqs. (2), (3) and (5) or Eqs. (6)–(11) was integrated by the method of lines [6]. The discretization of the integral form of Eq. (3) was achieved [7] by dividing the pellet into small volume elements (up to 50). The resulting system of ordinary differential equations was solved using backward differentiation formulas [8].

If necessary, transport parameters Ψ, $\langle r\rangle\Psi$ and $\langle r^2\rangle\Psi$ were obtained by minimization of objective function defined as sum of squares of deviations between calculated and experimentally determined relative pressures in the lower compartment, weighted by the number of experimental $p_{rel}(t)$ points. This weight was chosen because of different lengths of runs. The simplex algorithm of Nelder and Mead [9] minimized the objective function.

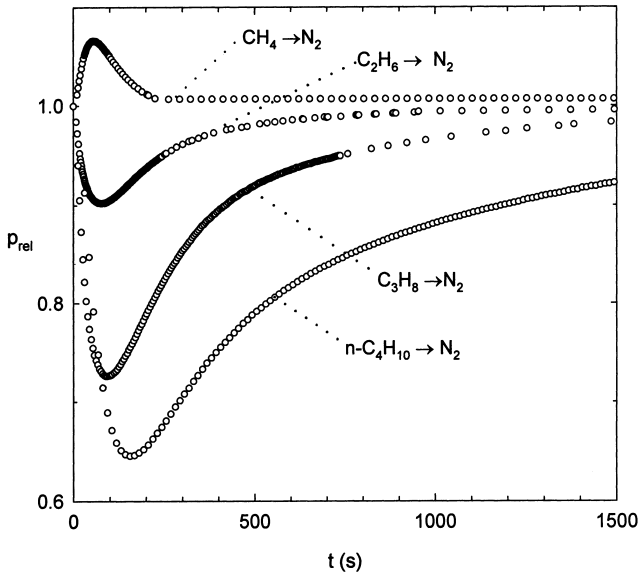

Fig. 4. Pressure responses of hydrocarbon→nitrogen binaries (adsorption mode). (In this and following figures only 5–20% of experimental points is shown).

4. Results and discussion

4.1. Binary systems

Fig. 4 summarizes pressure developments in the lower cell compartment for situation where hydrocarbon replaces nitrogen ($CH_4 \rightarrow N_2$,. . .,$C_4H_{10} \rightarrow N_2$; adsorption mode). The pressure change is a consequence of violation of the Graham law (12).[1]

$$\frac{N_1}{N_2} = -\sqrt{\frac{M_2}{M_1}}. \tag{12}$$

This law determines the ratio of fluxes of counter-currently transported gases, which must be satisfied under isobaric conditions. Under dynamic conditions the ratio of fluxes of transported components does not agree with this law. Hence, to satisfy the momentum balance of transported molecules a change in total pressure emerges. From Fig. 4 it is seen that the larger the difference in molecular weights of counter-currently transported species, the more pronounced the pressure change. Adsorption or desorption of a component results in a further flux increase which magnifies the deviation from the Graham law. Therefore, pressure changes are more pronounced for gases with higher adsorption equilibrium constants (which change similarly as molecular weights). With the exception of methane, the studied hydrocarbons have higher molecular weights than nitrogen. This causes an opposite pressure change with the binary $CH_4 \rightarrow N_2$ with $M(CH_4)<M(N_2)$ as seen in Fig. 4.

[1]The general form of Graham law follows from the constitutive equation (2) if the requirement of constant pressure is imposed.

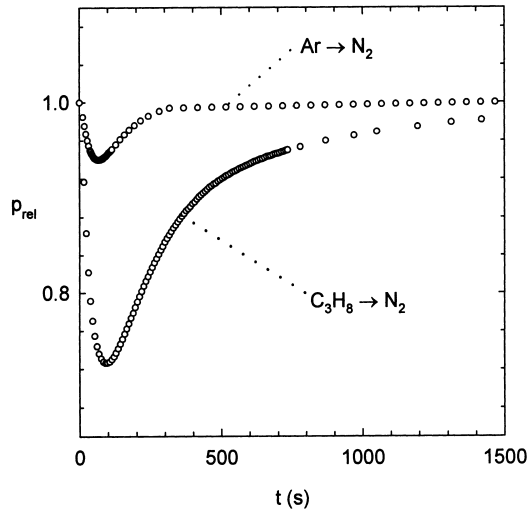

Fig. 5. Influence of adsorption on pressure responses ($Ar \rightarrow N_2$ and $C_3H_8 \rightarrow N_2$).

The role of adsorption of the transported component is demonstrated in Fig. 5. Here two gases with nearly identical molecular weights ($M(Ar) \approx 40$, $M(C_3H_8) \approx 44$) are counter-currently transported against nitrogen. The ability of propane to adsorb makes the maximum pressure decrease 6–7 times deeper than for the inert argon. Also the extreme pressure is arrived at longer time. The adsorption property is also illustrated (Fig. 6) by pressure responses of a mixture of propane and nitrogen with different content of propane replaced by pure nitrogen ($N_2 \rightarrow (C_3H_8+N_2)$). The pressure extremes decrease quite strongly with the increase of propane content in the ($C_3H_8+N_2$) mixture. The extreme position change is, however, only minor.

Similarly as with inert binary systems [1], the pressure responses for B→A pairs are not precise mirror images of the reversed systems A→B. Adsorption increases the dif-

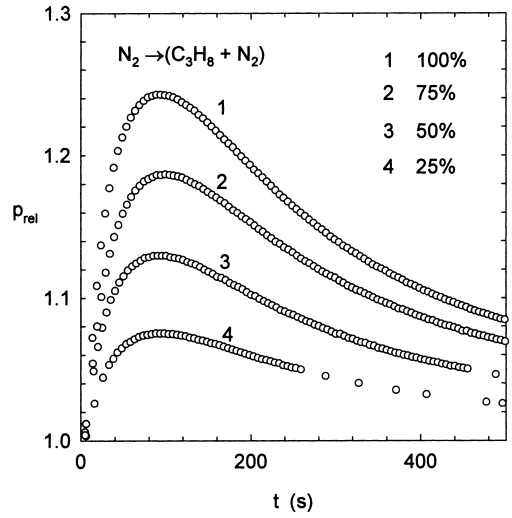

Fig. 6. Influence of propane concentration on $N_2 \rightarrow (C_3H_8+N_2)$ pressure response (desorption mode).

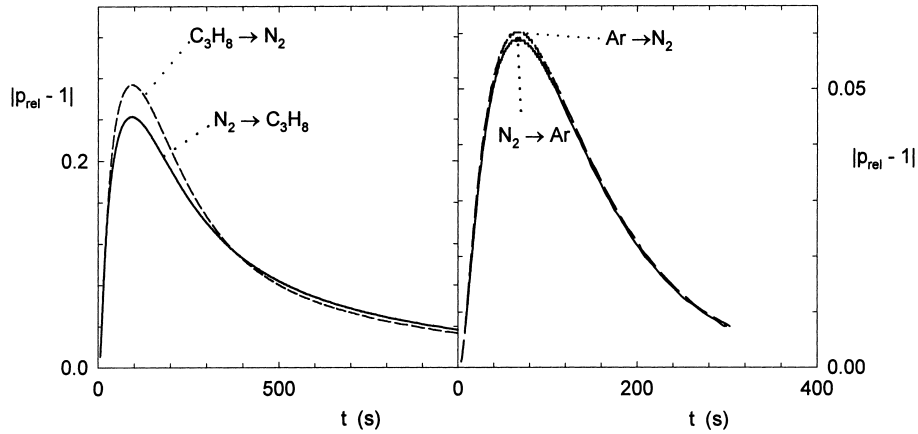

Fig. 7. Asymmetry of pressure responses for propane–nitrogen (adsorption and desorption modes) and argon–nitrogen.

ference as seen in Fig. 7 which compares the mirror images for an inert pair $Ar \rightarrow N_2$ and a pair containing adsorbable component $C_3H_8 \rightarrow N_2$ (in the form $|p_{rel} - 1|$ vs. t). The difference in pressure extremes in the system with propane is about 11% whereas in the purely inert case it is nearly an order of magnitude lower (1.6%).

4.2. Ternary systems

As an illustration, transport in the ternary system $H_2 \rightarrow (C_3H_8+N_2)$ with different C_3H_8/N_2 ratio in the $C_3H_8+N_2$ mixture is shown in Fig. 8. In general, the pressure responses follow similar trends as in binary systems. For intermediate contents of propane, pressure responses interpolate nearly linearly between the limiting responses for $H_2 \rightarrow N_2$ (0 vol% propane) and $H_2 \rightarrow C_3H_8$ (100 vol% propane).

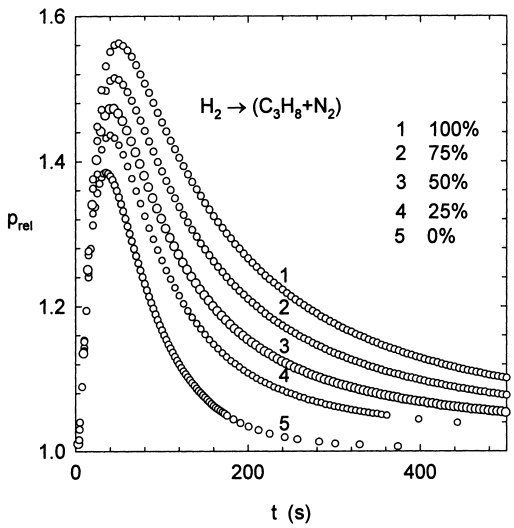

Fig. 8. Pressure responses for the ternary systems $H_2 \rightarrow (C_3H_8+N_2)$ (desorption mode). Curve parameters denote the percentage of propane in the $C_3H_8+N_2$ mixture.

4.3. Comparison of simulated and experimental pressure responses

Transport parameters of the ICI 52/1 catalyst were determined earlier by matching pressure responses of inert binary and ternary gases [1] and by a chromatographic method [10]. The obtained results are shown in Table 3 as sets I and II. In the chromatographic method no pressure gradients within the porous particles exists and parameter $\langle r^2 \rangle \Psi$, which characterizes the viscous flow, contribution is not accessible. Instead, $\langle r^2 \rangle \Psi$ was estimated as $(\langle r \rangle \Psi)^2/\Psi$ i.e assuming that $\langle r^2 \rangle = (\langle r \rangle)^2$. From matching of pressure responses of inert gases it appeared that the predominant transport mechanism is the Knudsen transport. Hence, parameters ψ and $\langle r^2 \rangle \Psi$ were not obtained.

Calculation of pressure responses was performed both for MTPM and DGM models. The differences between results was, however, always very small. Therefore, only the results for MTPM are presented.

First, it was assumed that the *adsorbed amount* of a component is *in equilibrium* with its pore concentration according to the Langmuir adsorption isotherm (4). The adsorption parameters were taken from Table 2 and ICI 52/1 transport parameters (obtained by fitting of pressure responses of inert gas pairs) from Table 3.

Table 3
Transport parameter of ICI 52/1 porous catalyst

Parameter	Method	
	Pressure response [1] [a]	Chromatographic [10]
	Set I	Set II
Ψ (dimensionless)	–	0.025
$\langle r \rangle \Psi$ (nm)	2.39	2.55
$\langle r^2 \rangle \Psi$ (nm^2)	$\rightarrow 0$	260 [b]

[a] Transport in Knudsen region.
[b] Estimated from $\langle r \rangle \Psi$ and Ψ.

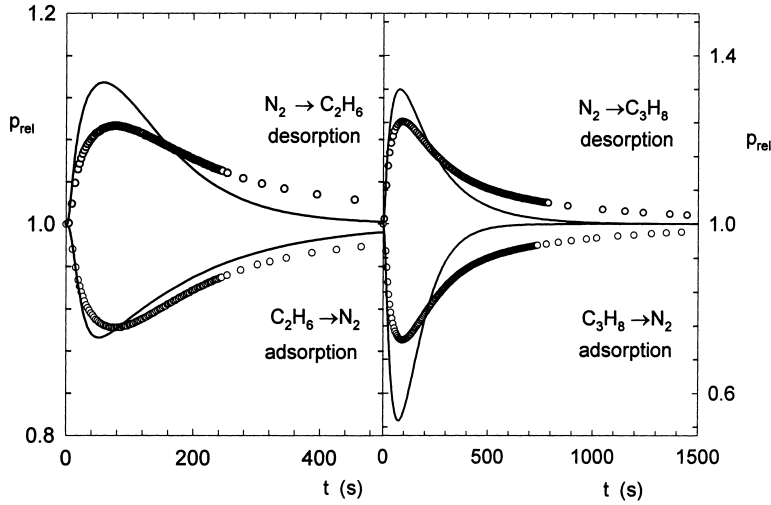

Fig. 9. Experimental and calculated pressure responses for adsorption equilibrium with transport parameters set I (Table 3). Points: experimental, line: calculated.

Fig. 9 shows that the agreement of calculations with experiments is not satisfying. Even though the general shape of experimental curves is reproduced, significant differences exist between calculations and experiments. Particularly, predictions for systems with *n*-butane (not shown in Fig. 9) are grossly in error. This can be caused, among other things, by capillary condensation of *n*-butane in pores. Saturated vapor pressure of *n*-butane at room temperature is about 200 kPa and with pure *n*-butane at atmospheric pressure the onset of capillary condensation (about 80 kPa) is reached at least in smaller pores. Numerical experiments have also shown that small changes of adsorption parameters cannot, in general, bring much better agreement between experiments and calculations.

Simulations based on both sets of transport parameters show always more prominent pressure response peaks than experimentally obtained. This can be caused by the assumption of equilibrium adsorption (i.e. very rapid process) due to which large fluxes of adsorbed species are generated. Such fluxes, then, violate the Graham law more, then in cases with inert gas pairs with the consequence of overestimating the height of the pressure response.

We have also tried to obtain transport parameters which would reproduce the experimental pressure responses by matching experiments with adsorbable gases to theory. The optimum parameters obtained in this way are summarized in Table 4. As can be seen, sets of transport parameters for individual systems differ and no unique set can be found which would be appropriate for all systems simultaneously. The inspection of the objective function also shows that the increase of deviations between experiments and calculations parallels the increase of hydrocarbon adsorption. Particularly, systems with *n*-butane show the highest deviations; here can capillary condensation play an additional role.

It is possible to weaken the assumption of adsorption equilibrium by considering the limited *rate of hydrocarbon*

Table 4
Transport parameters from pressure responses with adsorbable gases

Gas pair	Mode	(%) [a]	Ψ (dimensionless)	$\langle r\rangle\Psi$ (nm)	$\langle r^2\rangle\Psi$ (nm^2)	Objective function
$N_2 \rightarrow C_2H_6$	Desorption	–	0.027	1.89	0.0004	0.07
$N_2 \rightarrow C_3H_8$	Desorption	–	0.062	2.05	0.0014	0.77
$N_2 \rightarrow C_4H_{10}$	Desorption	–	0.070	0.97	0.0002	9.51
$C_2H_6 \rightarrow N_2$	Adsorption	–	0.014	1.88	0.0620	0.17
$C_3H_8 \rightarrow N_2$	Adsorption	–	0.016	2.19	0.0009	4.67
$C_4H_{10} \rightarrow N_2$	Adsorption	–	0.010	1.64	0.0001	62.43
$H_2 \rightarrow (C_2H_6+N_2)$	Desorption	25	0.148	2.41	0.0002	0.95
$H_2 \rightarrow (C_2H_6+N_2)$	Desorption	50	0.192	2.52	0.0586	1.63
$H_2 \rightarrow (C_2H_6+N_2)$	Desorption	75	0.109	2.29	0.0660	3.53
$(C_2H_6+N_2) \rightarrow H_2$	Adsorption	25	0.103	2.63	0.0082	2.68
$(C_2H_6+N_2) \rightarrow H_2$	Adsorption	50	0.089	2.76	0.1538	3.50
$(C_2H_6+N_2) \rightarrow H_2$	Adsorption	75	0.050	2.63	0.0007	11.51

[a] Amount of adsorbable component in mixture with nitrogen.

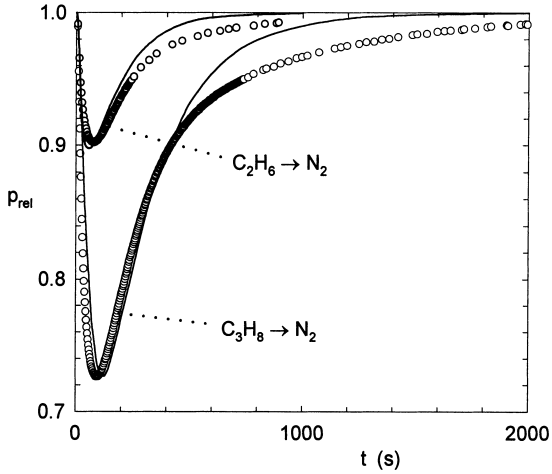

Fig. 10. Experimental and calculated pressure responses for $C_2H_6 \rightarrow N_2$ and $C_3H_8 \rightarrow N_2$ (adsorption mode) with adsorption kinetics (k_{ethane}=4.7 cm^3/mol s $k_{propane}$=10.9 cm^3/mol s). Points: experimental, line: calculated.

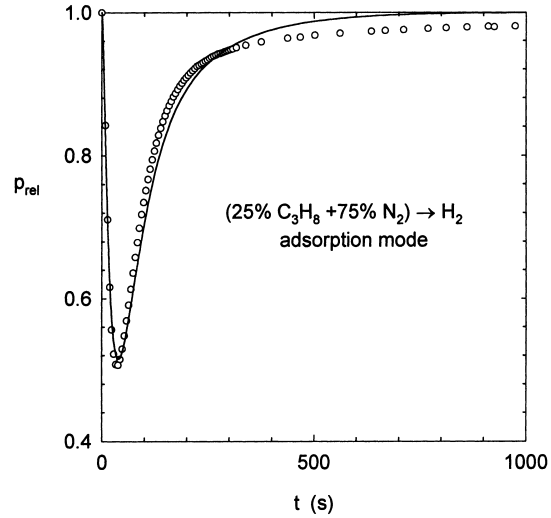

Fig. 11. Experimental and calculated pressure responses for (25% C_3H_8+75% N_2)→H_2 (adsorption mode) with adsorption kinetics ($k_{propane}$=10.9 cm^3/mol s). Points: experimental, line: calculated.

adsorption. Rough estimates[2] of adsorption rate constants, k_i, for ethane and propane were obtained from evaluation of adsorption kinetics in the course of equilibrium adsorption measurements (k_{ethane}=4.7 cm^3/mol s; $k_{propane}$=10.9 cm^3/mol s). Pressure responses for the adsorption mode of binary systems $C_2H_6 \rightarrow N_2$ and $C_3H_8 \rightarrow N_2$ calculated with these adsorption rate constants, adsorption equilibrium parameters (K_i, q_{max}) from Table 2 and transport parameter set I are depicted in Fig. 10. Apart from the response tails the agreement of prediction with experiment is satisfactory. Similar conclusion can be drawn for ternary systems; this illustrates the adsorption pressure response for a mixture (25% C_3H_8+75% N_2) which replaces hydrogen (Fig. 11).

Another possibility for pressure response simulation would be inclusion of an additional transport mechanism working in parallel with equilibrium adsorption, viz. *surface transport of adsorbed species*. This approach was employed by Tuchlenski et al. [10] who worked with Vycor glass membrane and used carbon dioxide and propane as adsorbable gases. It is worth noticing that in their case the mean transport pore radius determined as $\langle r \rangle \Psi/\Psi$ was (0.12/0.06=2 nm) about fifty times smaller than for the ICI 52/1 catalyst (2.55/0.025=102 nm). Surface diffusion was also considered by Do and Do [14] for multicomponent adsorption on activated carbon particles.

It seems, however, that in our case, consideration of such an additional transport mechanism would increase the fluxes with the consequence of increased deviations from the Graham law and increased pressure changes. This would bring the calculated pressure response even farther from our experiments.

[2]The set-up of Cahn vacuum microbalance is appropriate for equilibrium adsorption determinations where transport processes can be neglected. For adsorption kinetic measurements, such set-up is not completely suitable.

5. Conclusions

The dynamics of countercurrent transport of binary and ternary gas mixtures, containing inert gases (hydrogen, nitrogen) and one adsorbable gas (methane, ethane, propane, *n*-butane), through a porous industrial catalyst ICI 52/1, accompanied by a spontaneous temporary build-up of pressure inside the pores was experimentally studied. Time changes of pressure in the closed cell compartment (Fig. 1), similar in shape but more notable than with inert binary and ternary gas transport were observed. Attempts to simulate the pressure responses based on Maxwell–Stefan constitutive equation (2) were made with the conclusion that adsorption in equilibrium overpredicts the temporal pressure changes inside the pore structure. Acceptable simulation of pressure responses was achieved when adsorption kinetics was taken into account. It was argued that inclusion of surface diffusion of the adsorbable component would predict more marked pressure changes than experimentally determined.

6. Nomenclature

B_i	effective permeability coefficient
$\mathbf{c}$	vector of molar concentrations
c	total molar concentration of a gas mixture
c_i	molar concentration of component i
D_i^k	effective Knudsen diffusion coefficient
D_{ij}	effective bulk diffusion coefficient of pair i–j
$\mathscr{D}_{ij}$	binary bulk diffusivity of pair i–j
F	volumetric flow rate
$\mathbf{H}(\mathbf{c})$	$n \times n$ matrix
h_{ij}	elements of matrix $\mathbf{H}(\mathbf{c})$
k_i	adsorption rate constant of component i

K_i adsorption equilibrium constant of component i
Kn_i Knudsen number of component i
L pellet length
m number of adsorbable gases in the mixture
M molecular weight
$\mathbf{N}$ vector of molar flux densities
N_i molar flux density of component
n number of components in the gas mixture
p pressure: $p=cR_gT$
p_b atmospheric pressure
p_{rel} relative pressure
$\mathbf{q}$ vector of adsorbed amounts
q_i adsorbed amount of component i
q_{max} adsorption capacity
q_t tortuosity of transport pores
R_g gas constant
$\langle r\rangle$ mean transport pore radius
$\langle r^2\rangle$ mean of squared transport pore radii
S total cross-section of pellets mounted in the cell
T temperature
t time
V_L volume of lower cell compartment
V_U volume of upper cell compartment
x pellet length coordinate

Greek symbols

α,α_i parameters of MTPM and DGM, respectively
δ_{ij} Kroneker delta
ϵ_t porosity of transport pores
ν_i square root of relative molecular weight of gas mixture component i
Ψ geometric model parameter ($\Psi=\epsilon_t/q_t$)
ω numerical coefficient

Acknowledgements

The authors appreciate the financial support of this study by the Grant Agency of the Academy of Sciences of the Czech Republic (A472408).

Appendix A

The elements of matrix $\mathbf{H}(\mathbf{c})$ are defined as

$$h_{ii} = 1/D_i^k + (c_i\alpha_i/D_i^k) + \sum_{k=1}^{n}(c_k/cD_{ik}),$$

$$h_{ij} = c_i\alpha_i/D_j^k - c_i/(cD_{ij}) \quad i \neq j,$$

where D_{ij} is the effective bulk binary diffusion coefficient defined as $D_{ij}=\psi\mathscr{D}_{ij}$ and D_i^k is the effective Knudsen diffusion coefficient

$$D_i^k = (2/3)\langle r\rangle\Psi\sqrt{8R_gT/(\pi M_i)}.$$

The bulk binary diffusion coefficients, $\mathscr{D}_{ij}$, were taken from Marrero and Mason [11]. Differences between MTPM and DGM appear in the definition of parameter α_i:

For MTPM

$$\alpha_i = \left(1 - B_i/D_i^k - \sum_{k=1}^{n} c_k(B_i - B_k)/cD_{ik}\right) \Bigg/ \sum_{k=1}^{n} c_kB_k/D_k^k.$$

Here B_i is the effective permeability coefficient of mixture component i [12]:

$$B_i = D_i^k[(\omega\nu_i + Kn_i)/(1 + Kn_i)] + \langle r^2\rangle\Psi p/8\mu.$$

The numerical coefficient ω depends on the details of the wall-slip description (ω=0, 9, π/4, 3π/16, etc.; see [12]); ν_i is the square root of the relative molecular weight of the gas mixture component i:

$$\nu_i = \sqrt{M_i \Bigg/ \sum_{j=1}^{n} \frac{c_i}{c} M_j},$$

μ is the gas mixture viscosity and Kn_i is the Knudsen number of component i (mean free-path length of component i/transport pore diameter).

For DGM

$$\alpha_i = -(\beta/D_i^k) \Bigg/ \left(\sum_{k=1}^{n} c_k + \beta\sum_{k=1}^{n} c_k/D_k^k\right),$$

$$\beta = \langle r^2\rangle\Psi p/(8\mu).$$

The mixture viscosity μ depends on the mixture composition and was calculated from the Reichenberg's formula [13].

References

[1] P. Čapek, V. Hejtmánek, O. Šolcová, K. Klusáček, P. Schneider, Catal. Today 38 (1997) 31.
[2] V. Hejtmánek, P. Čapek, O. Šolcová, P. Schneider, Chem. Eng. J. 70 (1998) 189.
[3] P. Schneider, Chem. Eng. Sci. 33 (1978) 1311.
[4] M. Novák, K. Ehrhardt, K. Klusáček, P. Schneider, Chem. Eng. Sci. 43 (1988) 185.
[5] E.A. Mason, A.P. Malinauskas, Gas Transport in Porous Media: The Dusty Gas Model, Elsevier, Amsterdam, 1983.
[6] R.F. Sincovec, N.K. Madsen, ACM Trans. Math. Software 1 (1975) 261.
[7] K. Ehrhardt, K. Klusáček, P. Schneider, Comput. Chem. Eng. 12 (1998) 1151.
[8] A.C. Hindmarsh, ODEPACK, A systematic collection of ODE solvers, in: R.S. Stepleman et al. (Eds.), Scientific Computing, North-Holland, Amsterdam, 1983, pp. 55–64.
[9] D.M. Himmelblau, Nonlinear Programming, McGraw-Hill, New York, 1972, p. 148.
[10] A. Tuchlenski, P. Uchytil, A. Seidel-Morgenstern, J. Membr. Sci. 140(2) (1998) 165.
[11] T.R. Marrero, E.A. Mason, J. Phys. Chem. Ref. Data 1 (1972) 3.
[12] S. Weber, Dan. Mat. Fys. Medd. 28 (1954) 1.
[13] R.C. Reid, J.M. Prausnitz, B.E. Poling, The Properties of Gases and Liquids, McGraw-Hill, New York, 1988, p. 404.
[14] H.D. Do, D.D. Do, Chem. Eng. Sci. 53(6) (1998) 1239.